MATERIALS SCIENCE

Load-bearing entanglements in polymer glasses

Cynthia Bukowski[1†], Tianren Zhang[2†], Robert A. Riggleman[2]*, Alfred J. Crosby[1]*

Through a combined approach of experiment and simulation, this study quantifies the role of entanglements in determining the mechanical properties of glassy polymer blends. Uniaxial extension experiments on 100-nm films containing a bidisperse mixture of polystyrene enable quantitative comparison with molecular dynamics (MD) simulations of a coarse-grained model for polymer glasses, where the bidisperse blends allow us to systematically tune the entanglement density of both systems. In the MD simulations, we demonstrate that not all entanglements carry substantial load at large deformation, and our analysis allows the development of a model to describe the number of effective, load-bearing entanglements per chain as a function of blend ratio. The film strength measured experimentally and the simulated film toughness are quantitatively described by a model that only accounts for load-bearing entanglements.

INTRODUCTION

Glassy polymers, those below their glass transition temperature (T_g), are crucial to an expansive range of current and emerging technologies from additive manufacturing to filtration membranes for clean water. Their stiffness and processability make them attractive materials for many applications. Their strength, or the maximum stress a sample can withstand without failure, is decisive for determining lifetime and performance limits. The strength of polymer glasses has been studied classically, and it is broadly understood that entanglements between polymer molecules in the glassy state play a crucial role in the determination of strength (*1*). Below a critical number of entanglements per molecule, glassy polymer materials are excessively brittle and break at diminishing levels of stress (*2*, *3*). Above a critical entanglement density, polymer materials dissipate energy through intermolecular disentanglement and molecular scission to enhance their strength and toughness or the energy dissipated by deforming a sample to failure. These processes are unique to polymers and are a large reason for their wide-ranging use in many technologies. While entanglements are crucial for strength, they also necessitate the use of volatile solvents or excessive temperatures during the processing of glass-forming polymers. These practices are environmentally costly (*4*). Ideally, the minimal degree of entanglements could be known to design maximally strong polymer materials processed with minimal environmental cost. However, a molecular view of how polymer entanglements determine strength and toughness has not been fully developed, thus hampering the efficient design of polymer materials. Here, we combine new experimental capabilities with molecular dynamics (MD) simulations to reveal that not all entanglements contribute equally in a polymer glass. We develop and validate a scaling theory that describes the number of strength-contributing entanglements per polymer chain, thus providing a quantitative framework for maximizing strength with minimal entanglements in a polymer glass.

The mechanical properties of polymer glasses are controlled by the interplay of van der Waals forces and entanglements. Van der Waals forces between polymer segments dominate at low strains and temperatures, defining properties such as the elastic modulus, while entanglements dominate at large strains and high temperatures (*5*). The transition between these regimes is associated with the activation of mobile segments along the polymer chains, which controls the onset of yielding and subsequent permanent, or so-called plastic, deformation and failure. For polymer glasses, plastic deformation is often associated with the growth of crazes or shear deformation zones, both of which are localized deformation mechanisms that precede crack growth and ultimate failure. The morphology and growth mechanisms of both crazes and shear deformation zones have been studied extensively since the 1970s (*6*–*9*).

The role of entanglements in both crazes and shear deformation zones has been well established through experiments, simulations, and theory (*6*, *8*–*11*). Crazes form at low entanglement densities, and shear deformation zones form at high entanglement densities. The stability of a craze, or the resistance for a craze to break down and form a crack, is also a function of entanglement density, as well as temperature and strain rate (*12*). Many previous experimental studies have focused on understanding these deformation mechanisms, as they can be tracked morphologically with optical and transmission electron microscopy (*7*, *13*–*16*). A particularly attractive aspect of this approach is that it is conducive to using thin films, where model polymer blends of polymers with narrow polydispersity and controlled enthalpic interactions can be used to empirically isolate the role of molecular entanglements (*15*, *17*). However, linking these deformation mechanisms to the mechanical strength of a polymer glass is challenging since measurements of mechanical strength, such as the maximum failure stress or critical strain energy release rate, have been limited to thicker, bulk specimens where model polymer blends with controlled entanglements are challenging and cost prohibitive. In this study, we overcome this limitation by using a recently developed experimental method that allows measurement of the complete uniaxial stress-strain response of ultrathin polymer films (*16*, *18*). This approach allows us to systematically alter the state of entanglements using model polymer blends while also measuring their impact on mechanical strength.

MD simulations have provided valuable insights into the role of entanglements in the properties of polymer melts and glasses (*11*, *19*, *20*). Simulations of even simplified, coarse-grained glasses exhibit behaviors that agree very well with experiments during deformation close to T_g, where the response is ductile (*21*, *22*). However, there are

[1]Polymer Science and Engineering Department, University of Massachusetts Amherst, Amherst, MA 01003, USA. [2]Chemical and Biomolecular Engineering Department, University of Pennsylvania, Philadelphia, PA 19104, USA.
*Corresponding author. Email: rrig@seas.upenn.edu (R.A.R); acrosby@umass.edu (A.J.C.)
†These authors contributed equally to this work.

numerous challenges including the disparate length and time scales accessible to simulations and experiments, and the failure mode in common coarse-grained models is often ductile even at conditions where experiments expect brittle failure. Even at very low temperatures, the ductile response makes direct connection between the failure properties of glassy polymers in experiments and molecular simulations challenging. Below, we identify the appropriate quantities that describe mechanical strength in both MD simulations and experiments to realize quantitative connections between the two. This advance provides important opportunities for using predictive MD simulation studies to guide the design of more efficient polymer materials.

In addition to simulations, scaling theories have contributed to defining the role of entanglements in the mechanical properties of polymer glasses. Most theories have focused on understanding deformation mechanisms, such as crazes and shear deformation zones, and measurements of ductility, such as the maximum stretch ratio. These parameters and mechanisms can be connected to the morphological analysis approach afforded by thin films with controlled entanglement networks. Mikos and Peppas (*23*–*26*) developed predictive scaling models that focus on predicting the strength and toughness of polymer glasses, both of which are potentially more important for straightforward engineering design of materials. They approached the role of entanglements by developing a stochastic model based on effective crossings. An effective crossing is one in which two neighboring entanglements fall on opposite sides of a fracture plane, allowing the crossing chain to bear a load (*23*). This distinction excludes chain ends from being able to form entanglements. Counting the number of effective crossings per unit area, they postulate that fracture energy is controlled by the energy required to rupture all crossing molecules. In counting effective crossings, they consider two extremes of polydispersity, materials with monodisperse distributions of molecular length and polydisperse ones described by a Schultz-Flory distribution. The predicted difference between these two extremes is minor. For a polydisperse material, the fracture energy was proposed to obey $G_F = G_{F\infty} e^{\left(\frac{-2}{\langle Z \rangle}\right)}$, where $G_{F\infty}$ is the fracture energy for a polymer system with infinite molecular weight, $\langle Z \rangle \equiv M_n/M_e$, M_n being the number average molecular weight, and M_e the material-specific molecular weight between entanglements. For bulk specimens, which realistically have defects, the strength scales as $\sigma_F \sim \sqrt{\frac{E G_F}{L}}$ where E is the elastic modulus and L is the length of the largest defect. In the limit of zero defects, the strength is $\sigma_F = \sigma_{F\infty} e^{\left(\frac{-2}{\langle Z \rangle}\right)}$, where $\sigma_{F\infty}$ is the critical strength for an infinitely long chain. While these predictions for fracture energy and strength seemingly compared favorably to classical experimental data, these comparisons were made over ranges of molecular weights where it is difficult to resolve the accuracy of the chosen parameters, $G_{F\infty}$ and $\sigma_{F\infty}$ (*27*–*30*). While advantageous in many respects, these low-dispersity samples do not allow for understanding the role of various entanglements found in more typical polydisperse polymer materials. As we demonstrate below, the Mikos and Peppas theory does not accurately predict the behavior of bidisperse systems. Using the insight offered by MD simulations, we develop a modified theory that demonstrates that strength and fracture energy of polymer glasses are dictated by a predictable fraction of the interchain entanglements.

In this work, we use a combined experimental and MD approach to understand the role of entanglements on the deformation failure processes of thin glassy polymer blend films. The ability to directly quantify the far-field stress-strain response of model glassy polymer blend films provides a quantitative pathway to connect to MD simulation results. This approach allows us to examine both the macroscopic perspective of experimental films and the molecular perspective of local dynamics chain simulations to attain a multisize-scale understanding of polymer strength.

RESULTS

To control the number of entanglements in the system, we mixed monodisperse polymers of the same chemical structure. The monodisperse polymers have different molecular lengths including species that are much longer than M_e, species that are close to M_e, and species that are much less than M_e. In experiments, polystyrene of M_n = 150.9 kDa is mixed with either M_n = 13.7- or 59.5-kDa polystyrene. The M_e value used is 18.1 kDa (*23*). Simulations use a coarse-grained polymer model with chains of length or degree of polymerization, N = 250 combined with N = 10, 30, or 60 chains. For this model, the typical number of monomers between entanglements (N_e) is around 16. All simulation quantities are reported in reduced units scaled by the mass, van der Waals energy, and size of a polymer monomer. This blended method of sample preparation allows a wide range of the average number of entanglements per chain to be sampled, as the shorter chains dilute the longer chain's entanglement network (*15*, *17*).

In both experiments and simulations, various blend combinations are used where the volume fraction of long chain is represented by ϕ. In this manner, both the experiments and simulations are designed to provide quantitative insight into how the entanglement network contributes to the mechanical properties of glassy polymer materials (Fig. 1).

Mechanical properties of polymer blends

The measured mechanical response at various diluent concentrations with two different diluent lengths is shown in Fig. 2 for both simulations and experiments. As the concentration of the longest

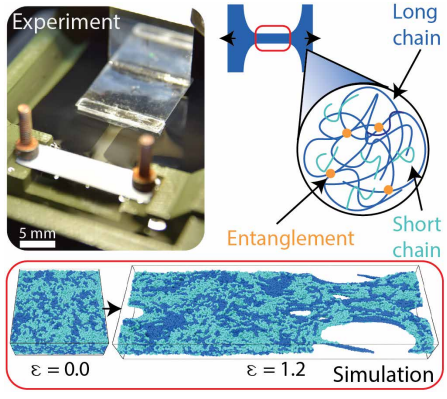

Fig. 1. Blended homopolymer thin films. Macroscopic experimental dog bone–shaped specimen (pictured) loaded in TUTTUT for uniaxial extension. Molecular-level simulations depict chains sliding past one another to form openings in the film as it is strained. Blended systems are composed of long (dark blue) and short (light blue) chains where most load-bearing entanglements (orange dots), if not all, are among the long polymer chains. Photo credit: C. Bukowski, University of Massachusetts Amherst.

chains is decreased, the maximum stress and failure strain begin to decrease for $\phi < 0.80$ in the experiments. In Fig. 2A, the representative curves for each blend demonstrate an initial linear elastic stress-strain response that plateaus after yield for larger ϕ values. Blends with $\phi > 0.80$ are dominated by the long chains in the system, and the short chains have little effect on the maximum stress. The plateaus in the curves indicate plastic deformation in the form of crazing. Crazes were observed with The Uniaxial Tensile Tester for Ultra-Thin (TUTTUT) films' in situ microscope across the gauge perpendicular to the axis of stretching for many measured samples with high ϕ. Lower ϕ value blends may have crazed locally around the failure location, but this location was not always in the microscope view and therefore, crazes cannot be confirmed for these blends. The blends with 13.7-kDa diluent only reach a dilution level of $\phi = 0.75$ before becoming too brittle to manipulate.

The experimental stress-strain curves in Fig. 2A resemble the low-strain regime of those simulated using blends of chains $N = 250$ and $N = 60$ or 30 in Fig. 2B. At the low-strain regime in the simulation stress-strain curves, there is an initial linear elastic region followed by a yield stress and postyield stress drop (see Fig. 2B, inset). After yielding, we observe different failure mechanisms by varying the degree of dilution (ϕ). There is a plastic plateau regime, followed by strain softening across most of the blend systems; we observe a strain hardening regime only for highly entangled systems ($\phi > 0.50$). The regimes exhibited in highly entangled systems are in qualitative agreement with a prior simulation study of crazing behavior in the bulk (*31*).

In the experimental results, a constant elastic modulus (E), within error, is observed across all blends (Fig. 2C). The measured moduli for polystyrene are comparable to literature values of bulk polystyrene specimens (*32*, *33*) and experimental values of thin films (*16*, *34*, *35*). The maximum stress σ_{Max} for blends with $\phi > 0.80$ is also approximately constant (Fig. 2D). When $\phi < 0.80$, the maximum stress decreases as a function of ϕ for both blended systems. The decrease observed in the 13.7-kDa diluted blends is higher than the 59.5-kDa blends.

The maximum stress in polystyrene is controlled by the craze propagation stress and the molecular weight (*2*). By blending chains, we are adding more chain ends to the sample, altering the average molecular length of the system, and continuously diluting our entanglement network (*15*, *17*). However, the maximum stress remains constant for undiluted and minimally diluted films, even as the addition of short chains is decreasing the total number of entanglements in the system. This suggests that not all entanglements bear load or are necessary to reach the maximum stress during a mechanical test.

The maximum stress begins to decrease after diluting films with more than 20 volume % (vol %) of short chains ($\phi < 0.80$), suggesting

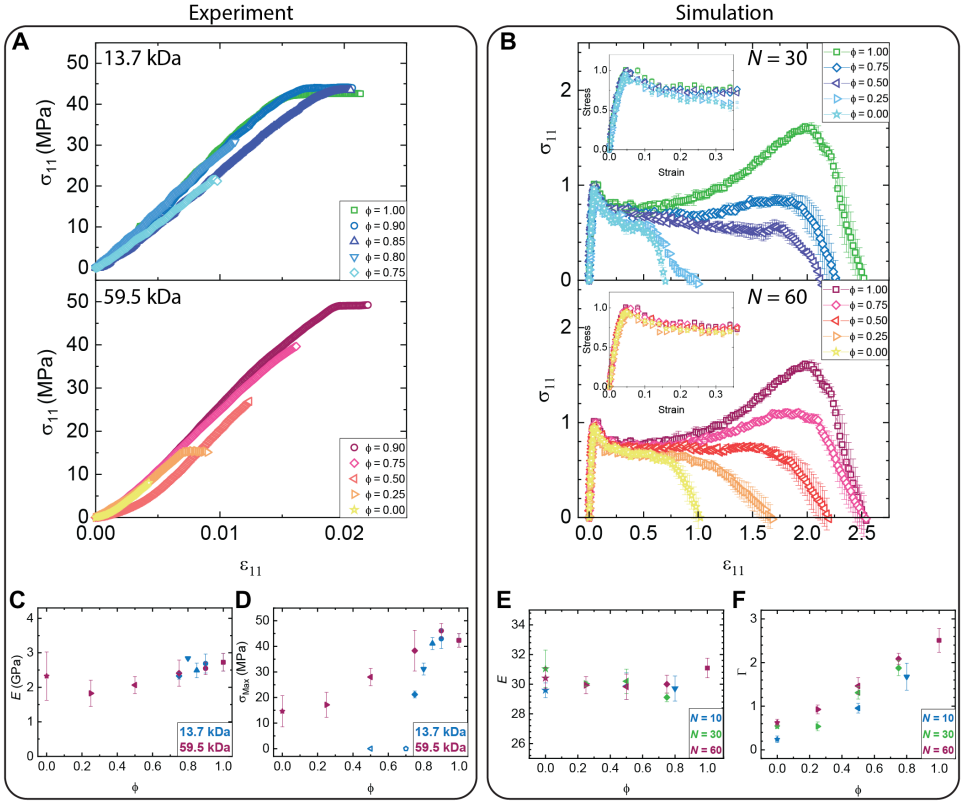

Fig. 2. Stress-strain behavior of polymer blends. (**A**) Representative uniaxial deformation stress-strain response for each blend tested experimentally on TUTTUT. ϕ represents the volume fraction of long chains in the system. The top graph is blends with 13.7 kDa as the short chain diluent and the bottom with 59.5 kDa. (**B**) Uniaxial deformation stress-strain responses of $N = 250$ ($\langle Z \rangle = 15.9$) blended with $N = 30$ (top) and 60 (bottom) at a temperature of $T/T_g = 0.71$. $\langle Z \rangle$ is 1.8 and 3.6 for each short chain, respectively. Low-strain response is included in the inset of each section. (**C**) The elastic modulus (E) for each experimentally measured blend. (**D**) The average maximum stress for each blend measured experimentally. Error bars are 1 SD of five to nine averaged films. Open symbols represent blends that were attempted but too brittle to manipulate in TUTTUT and stretch uniaxially. (**E**) The elastic modulus for each simulated blend. (**F**) The toughness value for each simulated blend.

that a critical number of entanglements necessary for achieving maximum strength is no longer present. This result is consistent with previous craze morphology measurements on polystyrene blends conducted by Yang *et al.* (*15*), who observed that the true stress in craze fibrils remains constant until a critical value of entanglement density is reached. However, connecting this craze fibril stress to the macroscopic strength has not been demonstrated previously. The Mikos and Peppas theory (*23*), discussed above, should quantitatively describe this development of strength above a critical number of entanglements, but a direct validation has yet to be demonstrated.

Compared to the experimental stress-strain curves, the results from simulations, where nonvolume conserving strains were applied, are much more ductile, and the strain at which films fail is orders of magnitude larger than experimental values. Simulated films with $\phi > 0.50$ exhibit strain hardening in strain regimes not achievable experimentally. These disparities in stress-strain response between experiment and simulation can be attributed to two main differences. First, there are known finite-size effects in the yielding and failure of simulated glasses (*36*), and certainly, the length scale of the simulation box is small compared to the large size scale of experimental specimens. To check the impact of size scale, we compared the stress-strain response of different simulation box sizes and observed a more rapid failure once the strain is above 0.3 in the larger sample (fig. S1), though this failure strain is still much higher than those in experiments. Second, there is a large difference in molecular friction between coarse-grained polymer models and real polymers. In simulations, failure only occurs through chain pullout. Assuming that a covalent bond should carry approximately 100 times the energy of a van der Waals bond to break, at no point do we observe any bond energies sufficiently large to merit consideration of chain scission. While the ratio of 100 is consistent with those expected from experiments (*37*) and numerous previous simulations (*38*, *39*), an additional possible source of the discrepancy could be the use of such a high ratio in a coarse-grained model. Experimentally, it is known that both failure modes, chain pullout and scission, play a role and that mechanically induced failure is highly defect dependent (*40*, *41*).

While these differences make direct comparisons between simulations and experiments challenging, we have identified the key parameters that allow quantitative connections to be made. In the glassy state, the elastic modulus is dictated by local intersegment interactions, dominated by van der Waals forces in the system studied here. Accordingly, trends of the elastic moduli as a function of entanglement density, or blend composition, should be comparable between experiments and simulations (Fig. 2, C and E, respectively). We see that both datasets have a constant elastic modulus across all blends measured. For failure related properties, the key parameters are the maximum stress for the experiments and the toughness for the simulations (Fig. 2, D and F, respectively). The maximum stress is dictated by the onset of local yielding processes associated with the onset of prefracture mechanisms, such as crazing. Consistent with classical models of yielding and crazing in polymer glasses, we anticipate that the energy barrier for this local process should scale with the work to failure, or toughness, measured in the simulations: $\Gamma = \int_0^{\varepsilon_{\sigma=0}} \sigma \, d\varepsilon$, where $\varepsilon_{\sigma=0}$ denotes the ε at which σ crosses zero in Fig. 2B. The toughness measured in the simulations reveals a monotonic increase, as more long chains ($N = 250$) are incorporated in the films, and blends with $N = 30$ are less tough than blends with $N = 60$ at the same ϕ (Fig. 2F).

Determining how to count entanglements

While the experimental maximum stress and simulated toughness values appear to scale differently, according to the Mikos and Peppas theory, the failure processes should scale with entanglement number, not blend volume fraction. Testing the Mikos and Peppas model with our data, we plotted normalized maximum stress and normalized toughness for the experiments and simulations, respectively, against the average entanglement number ($\langle Z \rangle$) in the system (Fig. 3). To determine $\langle Z \rangle$ in simulations, we used the *Z*1 algorithm to reduce our polymer configurations to the primitive path (PP) network, which is defined by straightening the polymer chains without allowing them to cross each other. At the end of the *Z*1 analysis, we are left with straight lines connecting the chain ends through a series of "kinks" where the chains bend around neighboring chains. We extract the mean number of interior kinks per chain to define $\langle Z \rangle$, which is proportional to the number of entanglements regardless of the details of the definition used to define an entanglement (*42*). Compared to the original Kremer-Grest (KG) model (*43*), the average number of monomers between entanglements

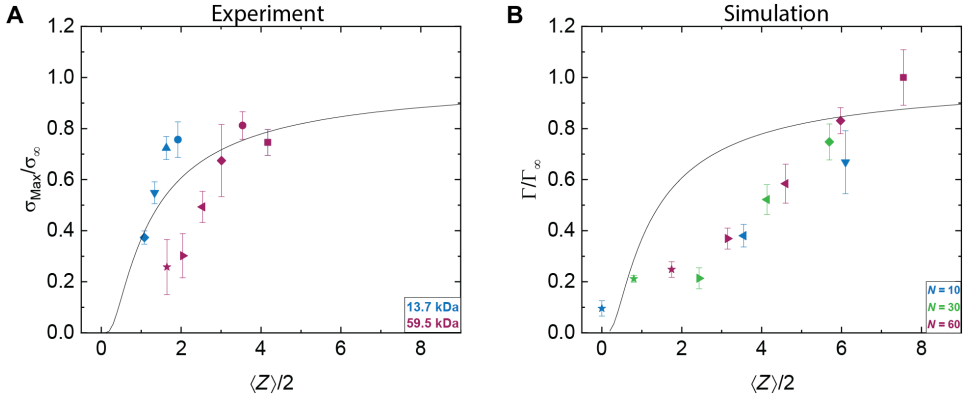

Fig. 3. Data plotted against the Mikos and Peppas model. Normalized experimental maximum stress, $\sigma_{Max}/\sigma_\infty$ (**A**), and normalized simulated toughness, Γ/Γ_∞ (**B**), as a function of entanglements, $\langle Z \rangle$. Here, $\langle Z \rangle$ is the M_n obtained from gel permeation chromatography of each blend divided by the M_e of polystyrene (18.1 kDa). For simulations, $\langle Z \rangle$ is average chain length *N* for each blend divided by N_e (*16*). Maximum stress and toughness are normalized by the maximum stress of polystyrene chains $M_n = 1.928$ MDa and the toughness of chains $N = 250$, respectively.

$\langle N_e \rangle$ is reduced in our systems due to the use of an angular potential, and more details on this are provided in Materials and Methods. $\langle Z \rangle$, experimentally, is calculated using the number average molecular weight of the blend system, the same average used by Mikos and Peppas, divided by M_e.

The maximum stress and toughness of each blend is normalized by the value measured for a system with an effectively infinite chain length (for experiments, M_n = 1.928 MDa; and for simulations, $N = 250$) and $\phi = 1$. Experimental measurements of M_n = 1.928 MDa are provided in fig. S2. The plotted normalized data should collapse onto a single exponential curve if in agreement with the model (Fig. 3). In Fig. 3, it is evident that the model does not adequately describe the experimental or simulation results. This finding indicates that the average entanglement number, $\langle Z \rangle$, does not accurately determine the failure properties of polymer glasses. To gain a better understanding of why this may be, we turned to simulations to observe local chain dynamics and determine differences among the entanglements in blended systems.

Simulations have shown that not all entanglements in a system are load bearing. For better visual representation, one long chain is selected from one of the blend films, and the monomers along the chain are color labeled by the average bond stress calculated in their corresponding PP (Fig. 4A) (*44*). A PP is the section of chain between the kinks that were generated by the *Z*1 algorithm described above. The first PP is from the end of a chain to the first entanglement. The second PP is from the first entanglement to the second entanglement, and this repeats until the center of the chain is reached. A schematic of each PP can be seen in Fig. 4B. The distribution of stress is heterogenous throughout the deformation, where some of the PPs internal to the chain (far from the chain end) carry more stress as the deformation proceeds. This is quantified in Fig. 4B, where the stress contribution from the PPs at different distances from the chain end shows that ends support much less load, on average, than the other sections further away from the ends. In addition, the average bond stress as a function of strain based on the monomer index for two individual blend systems is provided in fig. S3. These data support the earlier claim that not all entanglements in the entanglement network bear load. While the strains here are much larger than those seen experimentally, the increased bond stress toward the center of the chain supports the idea that stress on those entanglements is more likely to lead to chain scission at high strains in an experimental system, where molecular friction is higher. This finding supports the assumption of Mikos and Peppas, who did not include the chain end segments in determining the number of entanglements. However, as shown by the inability to describe both experimental and simulation results by their original theory (Fig. 3), a more complete counting of load-bearing entanglements is required.

When the total entanglement density (ρ) is calculated in simulations for varying dilution levels, blends with diluents where $N \geq N_e$ show that ρ remains constant, as seen in Fig. 4C. Here, ρ is calculated by dividing the total number of entanglements in the system by the volume. Removing the entanglements where either partner chain in the entanglement involves the first and second PPs shows that the "load-bearing entanglement density" decreases approximately linearly

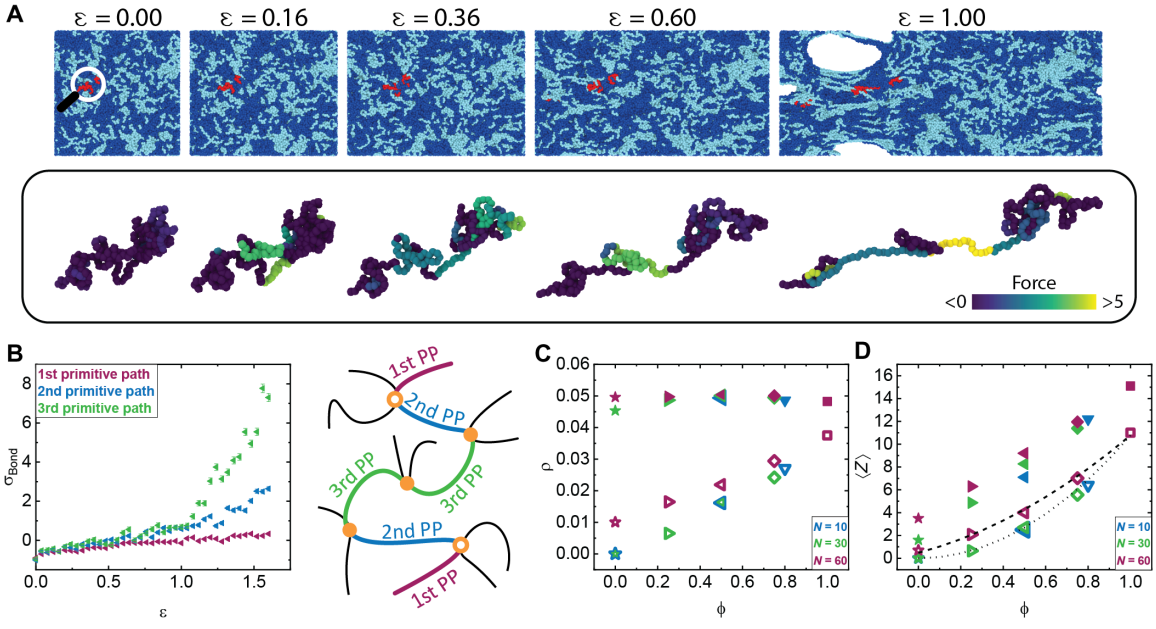

Fig. 4. Force distribution on entanglements. (**A**) Simulation snapshots at various levels of strain. A single chain, highlighted in red in the top row, is shown in the row below at each of the indicated strains. The single chains are colored to show varying levels of average bond stress on each primitive path (PP) along the chain. (**B**) The average bond stress as a function of strain on each PP in a blend of $N = 250$ and 30 at $\phi = 0.50$. The schematic next to the graph outlines where each mentioned PP is located. PPs are color coded to match the plotted points. Entanglements occur at each orange dot. Hollow orange dots represent non–load-bearing entanglements at the end of chains. (**C** and **D**) Solid symbols represent calculations that consider all entanglements in the blend systems, and hollow symbols only consider load-bearing entanglements. (C) The density of entanglements, ρ, in each simulated system as a function of dilution, calculated as the total number of entanglements divided by the system volume. Note that there is a solid blue star at point (0,0). (D) The average number of entanglements per chain, $\langle Z \rangle$, as a function of dilution. The dashed line corresponds to $N = 60$, and the dotted line corresponds to $N = 30$ as the diluent chain.

as a function of ϕ (hollow symbols in Fig. 4C). This trend in entanglement density is consistent with the previous empirical scaling that suggested the chain length between entanglements, N_e, increases for blends between long, entangled chains and short, unentangled chains: $N_e(\phi) = \frac{N_e(\phi = 1)}{\phi}$ (*45*, *46*). However, this proposed scaling does not capture the full trend, as the rate of increase between load-bearing entanglements and blend volume fraction depends on the length of the short-chain components (Fig. 4C).

To more precisely account for changes in load-bearing entanglements as the length of the short-chain component increases, we consider the average number of entanglements per chain in Fig. 4D. When all entanglements (load bearing and non–load bearing) are considered, the average number of entanglements per chain $\langle Z \rangle$ exhibits a linear relationship with ϕ. When we exclude the entanglement between the first and second PP and entanglements in the center of one chain whose partner is a chain end ($\langle Z_{eff} \rangle$), a nonlinear relationship between $\langle Z_{eff} \rangle$ and ϕ emerges. This dependence can be described by a mean field model that assumes that the chains are homogenously mixed and that the PPs near the chain ends do not contribute as load-bearing entanglements. The model is given by

$$\langle Z_{eff} \rangle = \left[\phi(Z_l - 2) + (1 - \phi)(Z_s - 2)\right] \times \left[\phi\left(\frac{Z_l - 2}{Z_l}\right) + (1 - \phi)\left(\frac{Z_s - 2}{Z_s}\right)\right] \quad (1)$$

where Z represents the number of entanglements per chain, and s and l correspond to short and long chains, respectively. The first bracketed part of the equation is a volume fraction weighted average of the mechanically effective number of entanglements per chains, and the second bracketed term represents the probability that those entanglements are formed with another mechanically effective entanglement. This second term was not considered in the development of the Mikos and Peppas theory, and we show that it accounts for the nonlinear coupling that is critical for properly determining entanglements that contribute to strength and toughness in polydisperse materials. For diluents too short to form entanglements, we treat the Z_s as 2 so that the load-bearing possibility is neglected. As indicated by the dashed lines (one is for diluents of $N = 60$ and one is for $N = 30$) in Fig. 4D, the mean-field model agrees very well with the number of effective entanglements per chain measured in simulations in the different blend systems. This model can be successfully applied to both experiments and simulations to study the relationship between entanglements and maximum stress or toughness, as shown in the next section. The experimental M_n values were measured for each blend using gel permeation chromatography (tables S1 and S2). For simulations, the average chain length was calculated for each simulated ϕ. The values used for chain length between entanglements are $M_e \approx 18.1$ kDa for experiments (*23*) and $N_e \approx 16$ for simulations (*47*).

Load-bearing entanglements only

Using the learned dependence of dilution on the entanglement network, we replot our experimental and simulated data and compare to a modified Mikos and Peppas model where we introduce two changes. First, we only account for entanglements that are load bearing, so $\langle Z \rangle \rightarrow \langle Z_{eff} \rangle$, and second, we allow for a nonzero strength (σ_0) and toughness (Γ_0) for systems without load-bearing entanglements ($\phi = 0$). The modified model is

$$\frac{\sigma_{Max}}{\sigma_\infty} = \left(1 - \frac{\sigma_0}{\sigma_\infty}\right) e^{\left(-\frac{2}{\langle Z_{eff} \rangle}\right)} + \left(\frac{\sigma_0}{\sigma_\infty}\right) \quad (2)$$

and

$$\frac{\Gamma}{\Gamma_\infty} = \left(1 - \frac{\Gamma_0}{\Gamma_\infty}\right) e^{\left(-\frac{2}{\langle Z_{eff} \rangle}\right)} + \left(\frac{\Gamma_0}{\Gamma_\infty}\right) \quad (3)$$

for the strength and toughness, respectively. The entire equation is normalized by maximum strength (σ_∞) and toughness (Γ_∞) of an infinitely long chain. Figure 5 shows both normalized experimental (solid symbols) and simulation (open symbols) data plotted as a function of only the load-bearing entanglements ($\langle Z_{eff} \rangle/2$). We observe that the data from both experiment and simulation overlap and show good agreement with the modified model, Eqs. 2 and 3, which are plotted as a solid and dotted line for the experiment and

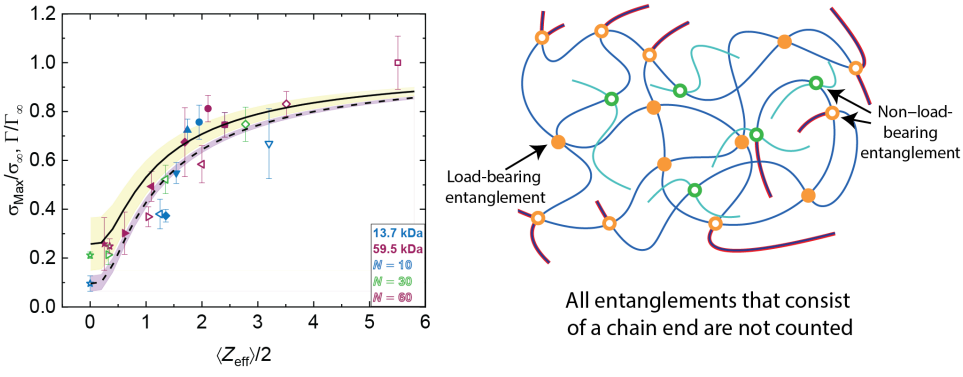

Fig. 5. Strength and toughness of materials as a function of load-bearing entanglements. Normalization is carried out by the undiluted maximum stress of polystyrene at $M_n = 1.928$ MDa and the undiluted toughness of $N = 250$ for the experimental and simulation results, respectively. Experimental data are represented by solid symbols, and simulation data are represented by hollow symbols. The lines represent the modified Mikos and Peppas model calculated for both the experiment (solid line) and simulation (dashed line) including only load-bearing entanglements. Each shaded region represents 1 SD of error in each line. The schematic on the right shows a system of entanglements with long chains (dark blue) and short chains (light blue). Solid orange dots represent load-bearing entanglements. Orange hollow dots represent entanglements that cannot bear load because they contain a first PP. Green hollow dots represent non–load-bearing entanglements that are made with a short species of chain. Ends of long chains are highlighted in red.

simulation, respectively. There are no fitting parameters in this comparison between the model and the data, only measured values averaged for multiple runs. The value for σ_0 is the maximum stress of 59.5-kDa polystyrene ($\phi = 0$), and Γ_0 is measured for chains of $N = 10$ ($\phi = 0$). The shaded regions represent 1 SD of the values used for σ_0, Γ_0, σ_∞, and Γ_∞ for each line. These results show that on a molecular level, both experiment and simulation scale in the same manner when considering the load-bearing fraction of entanglements in the system. The data also show a quantitative link between maximum stress and toughness when comparing experiment and simulation in thin glassy polymer films.

DISCUSSION

This work uses a combination of experiment and simulations to demonstrate the importance of considering load-bearing entanglements in the toughness of materials. By systematically tuning the entanglement density using bidisperse and chemically identical blends, tensile tests of polystyrene exhibit a decrease in maximum stress as a short-chain diluent is added, while MD simulations show a decrease in the toughness with added diluent. The microscopic analysis enabled by the simulations shows that entanglements between the first and second PP are unable to carry substantial stress at large deformation, and this leads to the development of a model to describe the number of effective, or load-bearing, entanglements as a function of the blend ratio. We find an exponential scaling between the film toughness in our simulations and the maximum stress in experiments when compared to the number of effective entanglements per chain. These findings match well with the model, which builds upon physics introduced by Mikos and Peppas, and now accounts for the load-bearing fraction of entanglements in polydisperse systems based on our results by accounting for chain ends in both chains involved in the formation of a potential entanglement. Our combination of experiments and simulations provides enhanced understanding of polymer failure on multiple length scales and provides a framework for tuning mechanical properties based on molecular makeup. In addition to the fundamental insights into the origin of toughness in polymer glasses, our results will also have practical implications for numerous technologies, most notably, in additive manufacturing, where droplets of polymer are deposited in sequence to build a three-dimensional structure, and the mechanical integrity of the structure depends on the formation of a tough interface between the two layers. Our results suggest that chains will need to diffuse multiple tube diameters to provide bulk-like mechanical support, although more detailed study of the consequences of our observations during interfacial healing would be necessary.

There are numerous differences between the simulations and experiments that remain to be addressed. While Mikos and Peppas (*23*) speculate in their work that their model should apply equally well to strength and toughness, a more concrete and theoretical connection between these mechanical properties is lacking. The ultimate failure mode may also be different in the simulations and experiments. While the presumed failure mode in the experiments is primarily through chain scission, the polymer chains in the simulations never experience a stress comparable to that expected to break a covalent bond. Whether this distinction is due to the rapid quenching used in the simulations or to the coarse-grained model with its reduced friction remains unclear. Tests of our simulation model using breakable bonds (*48*) observed no bond scission, and the maximum energy of any bond during our simulations was observed to be approximately 60 times the Lennard-Jones (LJ) bond strength, which is less than the energy needed to break a covalent bond. It may be that the ratio expected in coarse-grained models should be reduced and that will lead to a similar failure mode in simulations and experiments, but this remains an outstanding question. Last, it is known that failure in polymer glasses can be seeded near defects and contaminants that are necessarily present in experiments performed outside of a cleanroom. While the simulations are "clean," the small length scales of the simulated samples may also lead to differences in the failure mode (*36*).

MATERIALS AND METHODS

Materials

Polystyrene with an M_n of 150.9 kDa [weight-average molecular weight (M_w) = 157.2 kDa and polydispersity index (PDI) = 1.04] was obtained from Scientific Polymer Products Inc. The two short-chain species are polystyrene M_n = 59.5 kDa (M_w = 70.7 kDa, PDI = 1.19; Scientific Polymer Products Inc.) and monohydroxy-terminated polystyrene M_n = 13.7 kDa (M_w = 14.2 kDa, PDI = 1.04; Polymer Source). The invariant degree of polymerization $\sqrt{N}$ is ~68.4, 43, and 20.6 for M_n = 150.9, 59.5, and 13.7 kDa, respectively. Each of the above polymers' glass transition temperature was measured with differential scanning calorimetry. Gel permeation chromatography was used to verify the molecular weight of each polymer above and each tested blend (both in the Supplementary Materials). Polystyrene of M_n = 1.928 MDa (M_w = 2.257 MDa and PDI = 1.17) was purchased from Scientific Polymer Products Inc. All materials were used as received.

Sample preparation

Blend samples of 100 nm thickness were prepared by spin coating [3000 revolutions per minute (rpm)] 2.5 vol % polystyrene in toluene solutions onto freshly cleaved mica substrates. Films were then vacuum annealed in a 170°C oven for 25 min and cooled to room temperature at 0.4°C per min. Polystyrene films of 1.928 MDa required spin coating at 4000 rpm from a 1.5 vol % polystyrene in toluene solution to achieve the same thickness as the blended samples and were annealed for 24 hours at 170°C under vacuum. After annealing, a dog-bone shape was cut into the film using a laser (laser wavelength: 10.6 μm, infrared; Universal Laser Systems ULS3.50) at 3% power, 40% speed, and 706 points per inch.

TUTTUT experiments

Samples were floated off into TUTTUT's reverse osmosis water bath for uniaxial testing. They were subject to a strain rate of 0.0077 s^{-1}. Between five and nine samples for each blend were measured. Film thickness was measured by ellipsometry (refractive index = 1.59) in eight locations and averaged. Further details about the TUTTUT instrument can be found in previous work (*16*, *18*). In a previous study, measurements of freestanding films of polystyrene have been compared to those of water-supported films using the same instrument that we used in this current study. The only difference observed was that water acts as a craze stabilizer, enhancing the breaking strain slightly (*34*). Accordingly, we do not anticipate a water effect on the comparisons and conclusions made in the current study.

Simulation design

Our MD simulations used a modified version of the coarse-grained bead-spring KG model (*43*), where nonbonded monomers interact through the LJ potential

$$(U_{ij})^{nb} = 4\varepsilon\left[\left(\frac{\sigma}{r}\right)^{12} - \left(\frac{\sigma}{r}\right)^{6}\right] - 4\varepsilon\left[\left(\frac{\sigma}{r_{cut}}\right)^{12} - \left(\frac{\sigma}{r_{cut}}\right)^{6}\right] \quad (4)$$

for $r \leq r_{cut} = 2.5\sigma$. All the units were made dimensionless using the potential strength, ε; the monomer size, σ; and the unit time, $\tau = \sigma\left(\frac{m}{\varepsilon}\right)^{\frac{1}{2}}$, where m is the monomer mass. The bonded interactions connecting two successive monomers were governed by a finitely extensible nonlinear elastic potential with $k = \frac{30\varepsilon}{\sigma^2}$ and $R_0 = 1.5\sigma$. This bond type does not allow bond breaking during the uniaxial deformation process. We additionally added an angular harmonic potential of the form $U_{ang} = \frac{K_\theta}{2}(\theta - \theta_0)^2$ where $K_\theta = 10$ per radian^2 is the strength of this interaction and $\theta_0 = 120$ is the equilibrium bond angle (*47*). The angular potential, which is not in the original KG model, was introduced to increase the average number of entanglements per chain without having very long–polymer chain lengths, and the resulting average number of monomers between the entanglements is $\langle N_e \rangle \approx 16$. The number of monomers per chain in our simulations were $N = 10$, 30, 60, or 250, with N/N_e approximately equal to 0, 1.8, 3.75, and 15.9, respectively. Binary polymer blends were constructed by incorporating short chains $N = 10$, 30, or 60, which are treated as diluents, into long-chain $N = 250$ systems at thickness $H = 20\sigma$. The invariant degree of polymerization $\sqrt{N}$ is ~44.7, 18.9, 13, and 7.2 for $N = 250$, 60, 30, and 10, respectively. The simulation box size was $70\sigma \times 70\sigma \times H$, with a density of the system $\sim 0.85/\sigma^{-3}$ in the melted state. The free-standing films were generated by random growth of polymers in the simulation box with walls on the top and bottom, and soft potentials were applied to push the overlapped monomers away from each other. Next, the walls were removed to create free-standing films along the z direction, which was normal to the film. We note that our $N = 250$ chains have an equilibrium end-to-end distance of approximately 23.6σ, so we only expect minimal changes to the chain conformations due to confinement (*49*, *50*). In addition, the calculated elastic modulus, E, from the stress-strain curve is in reduced units from our simulations. It has the units of ε/σ^3, where ε and σ are the LJ parameters of a polymer monomer. To convert to real units, we chose our length scale to be $\sigma \approx 1$ nm, and the energy scale is taken from the glass transition $\varepsilon = k_B T_{g,expt}/T_{g,sim}$. Using our simulated $T_g \approx 0.6$ and $T_{g,expt} = 400$ K to correspond to a very high cooling rate, our dimensionless Young's modulus of $E_y \approx 30$ corresponds to approximately 0.3 GPa in laboratory units, which is in reasonable agreement with the expected magnitude of gigapascal moduli.

To accelerate the equilibration of the free-standing thin film systems, connectivity-altering Monte Carlo moves were applied in the simulations (*51*–*53*). The equilibration proceeded with a time step of $\Delta t = 0.002\tau$ until we observed diffusive behavior of the center of mass mean squared displacement (MSD), and the MSD was calculated with a moving time origin to improve the statistics. Three independent configurations of the films for each system were generated at high temperatures, and we then cooled those polymer films from $T = 1.0\left(\frac{T}{T_g} = 1.67\right)$ to $T = 0.4\left(\frac{T}{T_g} = 0.67\right)$ at a cooling rate of $\Delta T/\Delta t = 0.1$ per 2000τ to generate our glassy polymer thin films. Subsequently, we deformed each film under a constant temperature at a constant true rate $\dot{\varepsilon} = 1 \times 10^{-4}$ by applying uniaxial tension in the x direction. All the simulations were performed with Large-scale Atomic/Molecular Massively Parallel Simulator MD simulation package with the Velocity Verlet algorithm and a Nosé-Hoover thermostat (*54*). Canonical ensemble (NVT) ensemble with periodic directions x and y was used for all the processes. We note that the nonperiodic direction (z) is free to exhibit fluctuations in thickness and contract during deformation, and hence the sample behaves as though it is held at a constant pressure of 0 in the z direction.

SUPPLEMENTARY MATERIALS

Supplementary Material for this article is available at https://science.org/doi/10.1126/sciadv.abg9763

REFERENCES AND NOTES

1. R. S. Porter, J. F. Johnson, The entanglement concept in polymer systems. *Chem. Rev.* **66**, 1–27 (1966).
2. J. F. Fellers, B. F. Kee, Crazing studies of polystyrene. I. A new phenomenological observation. *J. Appl. Polym. Sci.* **18**, 2355–2365 (1974).
3. J. F. Fellers, T. F. Chapman, Deformation behavior of polystyrene as a function of molecular weight parameters. *J. Appl. Polym. Sci.* **22**, 1029–1041 (1978).
4. S. H. Patel, M. Xanthos, Environmental issues in polymer processing: A review on volatile emissions and material/energy recovery options. *Adv. Polym. Technol.* **20**, 22–41 (2001).
5. J. D. Ferry, The Plateau and Terminal Zones in Uncross-linked Polymers, in *Viscoelastic Properties of Polymers* (Wiley, ed. 3, 1980), pp. 366–403.
6. B. D. Lauterwasser, E. J. Kramer, Microscopic mechanisms and mechanics of craze growth and fracture. *Philos. Mag. A* **39**, 469–495 (1979).
7. T. Chan, A. M. Donald, E. J. Kramer, Film thickness effects on craze micromechanics. *J. Mater. Sci.* **16**, 676–686 (1981).
8. A. M. Donald, E. J. Kramer, The competition between shear deformation and crazing in glassy polymers. *J. Mater. Sci.* **17**, 1871–1879 (1982).
9. A. M. Donald, E. J. Kramer, Molecular weight distribution effects on craze micromechanics. *Polymer* **24**, 1063–1066 (1983).
10. J. Hyon, O. Lawal, O. Fried, R. Thevamaran, S. Yazdi, M. Zhou, D. Veysset, S. E. Kooi, Y. Jiao, M. S. Hsiao, J. Streit, R. A. Vaia, E. L. Thomas, Extreme energy absorption in glassy polymer thin films by supersonic micro-projectile impact. *Mater. Today* **21**, 817–824 (2018).
11. T. Ge, C. Tzoumanekas, S. D. Anogiannakis, R. S. Hoy, M. O. Robbins, Entanglements in glassy polymer crazing: Cross-links or tubes? *Macromolecules* **50**, 459–471 (2017).
12. E. J. Kramer, Craze fibril formation and breakdown. *Polym. Eng. Sci.* **24**, 761–769 (1984).
13. C. S. Henkee, E. J. Kramer, Loss of entanglement density during crazing. *J. Mater. Sci.* **21**, 1398–1404 (1986).
14. L. L. Berger, E. J. Kramer, The effect of temperature on the transition from crazing to shear deformation in crosslinked polystyrene. *J. Mater. Sci.* **23**, 3536–3543 (1988).
15. A. C. M. Yang, E. J. Kramer, C. C. Kuo, S. L. Phoenix, Crazes in diluted entanglement networks of polystyrene. *Macromolecules* **19**, 2020–2027 (1986).
16. R. K. Bay, S. Shimomura, Y. Liu, M. Ilton, A. J. Crosby, Confinement effect on strain localizations in glassy polymer films. *Macromolecules* **51**, 3647–3653 (2018).
17. J. D. McGraw, K. Dalnoki-Veress, Swelling molecular entanglement networks in polymer glasses. *Phys. Rev. E* **82**, 1–5 (2010).
18. Y. Liu, Y. C. Chen, S. Hutchens, J. Lawrence, T. Emrick, A. J. Crosby, Directly measuring the complete stress-strain response of ultrathin polymer films. *Macromolecules* **48**, 6534–6540 (2015).
19. R. S. Hoy, M. O. Robbins, Strain hardening in polymer glasses: Limitations of network models. *Phys. Rev. Lett.* **99**, 117801 (2007).
20. M. Warren, J. Rottler, Simulations of aging and plastic deformation in polymer glasses. *Phys. Rev. E* **76**, 031802 (2007).
21. R. A. Riggleman, H. N. Lee, M. D. Ediger, J. J. De Pablo, Heterogeneous dynamics during deformation of a polymer glass. *Soft Matter* **6**, 287–291 (2010).
22. H.-N. Lee, R. A. Riggleman, J. J. de Pablo, M. D. Ediger, Deformation-induced mobility in polymer glasses during multistep creep experiments and simulations. *Macromolecules* **42**, 4328–4336 (2009).
23. A. G. Mikos, N. A. Peppas, Polymer chain entanglements and brittle fracture. *J. Chem. Phys.* **88**, 1337–1342 (1988).
24. A. G. Mikos, N. A. Peppas, Polymer chain entanglements and brittle fracture: 2. Autohesion of linear polymers. *Polymer* **30**, 84–91 (1989).
25. A. G. Mikos, N. A. Peppas, Polymer chain entanglements and brittle fracture. III. Critical fracture strength of macromolecular materials. *J. Mater. Sci. Lett.* **8**, 833–834 (1989).
26. A. G. Mikos, N. A. Peppas, Brittle fracture of entangled polymers. *J. Polym. Sci. Part B Polym. Phys.* **29**, 837–841 (1991).

27. H. W. McCormick, F. M. Brower, L. Kin, The effect of molecular weight distribution on the physical properties of polystyrene. *J. Polym. Sci.* **39**, 87–100 (1959).
28. J. P. Berry, Fracture processes in polymeric materials. V. Dependence of the ultimate properties of poly(methyl methacrylate) on molecular weight. *J. Polym. Sci. A Gen. Pap.* **2**, 4069–4076 (1964).
29. R. P. Kusy, D. T. Turner, Influence of the molecular weight of poly(methyl methacrylate) on fracture surface energy in notched tension. *Polymer* **17**, 161–166 (1976).
30. R. P. Kusy, M. J. Katz, Effect of molecular weight on the fracture surface energy of poly(methyl methacrylate) in cleavage. *J. Mater. Sci.* **11**, 1475–1486 (1976).
31. J. Rottler, M. O. Robbins, Growth, microstructure, and failure of crazes in glassy polymers. *Phys. Rev. E* **68**, 011801 (2003).
32. W. Brostow, Mechanical Properties, in *Physical Properties of Polymers Handbook*, J. E. Mark, Ed. (Springer, New York, ed. 2, 2007), pp. 423–445.
33. M. F. Ashby, Materials selection charts, in *Materials Selection in Mechanical Design*, (Butterworth-Heinemann, ed. 2, 1999) pp. 32–64.
34. R. K. Bay, A. J. Crosby, Uniaxial extension of ultrathin freestanding polymer films. *ACS Macro Lett.* **8**, 1080–1085 (2019).
35. P. Yiu, H. Yuan, Q. Gu, P. Gao, O. K. C. Tsui, Strain rate and thickness dependences of elastic modulus of free-standing polymer nanometer films. *ACS Macro Lett.* **9**, 1521–1526 (2020).
36. Z. Zhang, S. Ispas, W. Kob, The critical role of the interaction potential and simulation protocol for the structural and mechanical properties of sodosilicate glasses. *J. Non Cryst. Solids* **532**, 119895 (2020).
37. C. Creton, E. J. Kramer, C. Y. Hui, H. R. Brown, Failure mechanisms of polymer interfaces reinforced with block copolymers. *Macromolecules* **25**, 3075–3088 (1992).
38. S. W. Sides, G. S. Grest, M. J. Stevens, Surface-tethered chains entangled in a polymer melt: Effects on adhesion dynamics. *Phys. Rev. E.* **64**, 050802 (2001).
39. J. Rottler, S. Barsky, M. O. Robbins, Cracks and crazes: On calculating the macroscopic fracture energy of glassy polymers from molecular simulations. *Phys. Rev. Lett.* **89**, 148304 (2002).
40. A. C. M. Yang, E. J. Kramer, C. C. Kuo, S. L. Phoenix, Craze fibril stability and breakdown in polystyrene. *Macromolecules* **19**, 2010–2019 (1986).
41. C. C. Kuo, S. L. Phoenix, E. J. Kramer, Geometrically necessary entanglement loss during crazing of polymers. *J. Mater. Sci. Lett.* **4**, 459–462 (1985).
42. R. S. Hoy, K. Foteinopoulou, M. Kröger, Topological analysis of polymeric melts: Chain-length effects and fast-converging estimators for entanglement length. *Phys. Rev. E* **80**, 031803 (2009).
43. K. Kremer, G. S. Grest, Erratum: Dynamics of entangled polymer melts: A molecular-dynamics simulation. *J. Chem. Phys.* **92**, 5057 (1991).
44. A. Stukowski, Visualization and analysis of atomistic simulation data with OVITO–the Open Visualization Tool. *Model. Simul. Mater. Sci. Eng.* **18**, 015012 (2010).
45. A. Sánchez-Valencia, O. Smerdova, L. R. Hutchings, D. S. A. De Focatiis, The roles of blending and of molecular weight distribution on craze initiation. *Macromolecules* **50**, 9507–9514 (2017).
46. E. J. Kramer, L. L. Berger, Fundamental Processes of Craze Growth and Fracture, in *Advances in Polymer Science Crazing in Polymers Vol. 2*, 91/92, H. H. Kausch, Ed. (Springer, 1990) pp. 1–68.
47. R. Kumar, M. Goswami, B. G. Sumpter, V. N. Novikov, A. P. Sokolov, Effects of backbone rigidity on the local structure and dynamics in polymer melts and glasses. *Phys. Chem. Chem. Phys.* **15**, 4604–4609 (2013).
48. T. Ge, F. Pierce, D. Perahia, G. S. Grest, M. O. Robbins, Publisher's Note: Molecular dynamics simulations of polymer welding: Strength from interfacial entanglements [Phys. Rev. Lett. **110**, 098301 (2013)]. *Phys. Rev. Lett.* 110, 129902 (2013).
49. N.-K. Lee, D. Diddens, H. Meyer, A. Johner, Local chain segregation and entanglements in a confined polymer melt. *Phys. Rev. Lett.* **118**, 067802 (2017).
50. D. M. Sussman, W.-S. Tung, K. I. Winey, K. S. Schweizer, R. A. Riggleman, Entanglement reduction and anisotropic chain and primitive path conformations in polymer melts under thin film and cylindrical confinement. *Macromolecules* **47**, 6462–6472 (2014).
51. S. W. Sides, G. S. Grest, M. J. Stevens, S. J. Plimpton, Effect of end-tethered polymers on surface adhesion of glassy polymers. *J. Polym. Sci. Part B Polym. Phys.* **42**, 199–208 (2004).
52. V. G. Mavrantzas, T. D. Boone, E. Zervopoulou, D. N. Theodorou, End-bridging Monte Carlo: A fast algorithm for atomistic simulation of condensed phases of long polymer chains. *Macromolecules* **32**, 5072–5096 (1999).
53. B. J. Banaszak, J. J. de Pablo, A new double-rebridging technique for linear polyethylene. *J. Chem. Phys.* **119**, 2456–2462 (2003).
54. S. Plimpton, Fast parallel algorithms for short-range molecular dynamics. *J. Comput. Phys.* **117**, 1–19 (1995).

Acknowledgments: We thank R. K. Bay and K. Dalnoki-Veress for their helpful discussions. **Funding:** This work was primarily supported by NSF DMR 1904776 and DMR 1904525. Preliminary data were collected during NSF DMR 1608614. The computational work used the Extreme Science and Engineering Discovery Environment (XSEDE), which is supported by NSF ACI-1548562, accessed through allocation TG-DMR 150034. **Author contributions:** C.B. carried out experimental measurements of blends and analyzed experimental results. T.Z. conducted simulations of glassy blends and analyzed simulation data. C.B. and T.Z. contributed to figure preparation. A.J.C. and R.A.R. supervised and oversaw the project. All authors contributed to the writing of the manuscript and participated in discussions of the research. **Competing interests:** The authors declare that they have no competing interests. **Data and materials availability:** All data needed to evaluate the conclusions in the paper are present in the paper and/or the Supplementary Materials. Data are available through UMass Amherst ScholarWorks (https://scholarworks.umass.edu/data/137/).

Submitted 16 February 2021
Accepted 29 July 2021
Published 17 September 2021
10.1126/sciadv.abg9763

Citation: C. Bukowski, T. Zhang, R. A. Riggleman, A. J. Crosby, Load-bearing entanglements in polymer glasses. *Sci. Adv.* **7**, eabg9763 (2021).

Load-bearing entanglements in polymer glasses

Cynthia BukowskiTianren ZhangRobert A. RigglemanAlfred J. Crosby

Sci. Adv., 7 (38), eabg9763. • DOI: 10.1126/sciadv.abg9763